INTERNATIONAL JOURNAL OF AUTOMOTIVE AND MECHANICAL ENGINEERING
ISSN: 2229-8649 e-ISSN: 2180-1606
VOLUME 23, ISSUE 3, 2026, 13816 - 13831
DOI: https://doi.org/10.15282/ijame.23.3.2026.6.1042

RESEARCH ARTICLE

Transient thermal efficiency enhancement of gasoline turbocharged direct injection engines using intake manifold air boosting assistance

Momen Sughayyer

Department of Mechanical Engineering, Palestine Polytechnic University, P726, Hebron, Palestine

Abstract - Improving drivability performance requires enhancing the typical thermal efficiency and power output of the engine during transient maneuvers, which depends highly on the cylinder contents. To achieve the required improvement, an investigation of the intake manifold air-boosting assistance for turbocharged direct-injection gasoline engines was considered. Comprehensive modeling of vehicle powertrains for evaluating common low- to medium-load and speed transients was adopted in this study. The model includes gas-exchange processes, turbocharger response, and vehicle dynamics, particularly during the lean stratified mode. This allows the evaluation of possible improvements to the common low- to medium-speed vehicle dynamics that represent urban driving conditions. Thus, it helps enforce a global intermediate green transition. A four-stroke, four-cylinder engine was used for this purpose, including the vehicle specifications. The adopted air-boosting assistance technique was simple and innovative. This allows for an accurate representation of the in-cylinder charge density variations of current internal combustion engine technologies, including those using e-fuels and hybrid powertrains. To that end, the results demonstrate how thermal efficiency can be enhanced during engine transients using air boosting in the intake manifold, immediately realizing a high boost pressure (1.75-2.25 bar) and reducing turbo lag by increasing the trapped mass (3.1-4.9 gm). Under various engine speeds (1000-3000 rpm) and load conditions, the results show significant improvements in the mean effective pressure and torque due to high-pressure boosting assistance but moderate changes in thermal efficiency while maintaining engine power and torque output. Effectively, demonstrated improved performance with environmental benefits.

Article History
Received : 31 August 2025
Revised : 26 June 2026
Accepted : 29 July 2026
Published : 25 September 2026

Keywords
Drivability performance
Thermal efficiency
Manifold air boosting
GTDI Engines
Powertrain modeling

1. Introduction

The need to improve vehicle drivability performance requires the development of innovative technical solutions to increase the efficiency and power output of current powertrain technologies during common driving maneuvers. Simultaneously, it is important to align with global efforts to reduce emissions in the near- and mid-term future. The IEA [1] reports that total transport carbon emissions from fuel combustion will grow by approximately 0.5% in 2025. Even with the deployment of renewable energy technologies and electric vehicles, the annual global fossil fuel energy demand is increasing; approximately half of the electricity production relies on fossil fuels to meet the additional electricity demand. Moreover, the ICCT [2] reports that the automotive industry trend of producing more Sport Utility Vehicle models, which are powered mainly by ICEs, due to market demand, has led to a surge in CO_2 emissions. Therefore, innovative solutions to enhance the efficiency of current ICE technologies are required to balance long- and short-term environmental impacts. Such solutions come with positive socio-economic effects, given that they help societies gradually adapt their capabilities to use electric vehicles, despite high ownership costs and the lack of energy infrastructure, laws, and policies. To improve the performance of road vehicles in the near- and mid-term future, this study addresses the improvement of ICE's thermal efficiency of ICEs, which positively impacts energy consumption and carbon emissions. Gasoline Turbocharged Direct Injection (GTDI) engines (technically called Turbocharged Stratified Injection or Turbo Fuel Stratified Injection) are widely adopted to improve part-load operation for urban driving fuel economy and hybrid powertrains. Thus, it was considered for possible thermal efficiency improvement in this study.

For this purpose, the intake manifold air-boosting-assistance technique was considered to improve the transient efficiency of GTDI engines, which is a crucial factor in enhancing the dynamic performance of vehicles during low-power-range transients. Thus, it supports the engine downsizing trend and carbon emissions reduction. Given that ICEs typically require fuel enrichment during acceleration, which increases fuel consumption and carbon emissions, this contribution primarily targets accelerations within the low-load/low-speed driving ranges. This range is characterized by low efficiency, especially under common urban driving conditions, even when the engine operates in stratification mode. Such engine performance occurs when the conditions of low manifold pressure and turbo lag are realized. Thus, it prevents the achievement of higher efficiency values. Over the last two decades, this approach has attracted many researchers, and their results have been published in several scientific and technical articles. Published contributions widely target the engine downsizing of throttled Spark Ignition (SI) engines using intake manifold boosting. Zsiga et al. [3] used turbo-lag compensation with intake manifold boosting for a load step from 1.7 to 16.7 bar BMEP at 2000 rpm to reduce the transient time from 2.8 s to 124 ms using 11.8 g of pressurized air, which did not include the lower-efficiency engine speeds. Mamala et al. [4] observed significant improvement in driving force during the first phase of the acceleration test for a vehicle equipped with a throttled SI engine, which requires increasing fuel quantity to maintain mixture combustibility and opposes lean combustion trends. Lefebvre and Guilain [5] used an e-booster to increase the air mass flow in the compressor to improve the engine response during vehicle acceleration; the response time was reduced from 3.0 s to 1.0

*CORRESPONDING AUTHOR | M. Sughayyer | ✉ sughayyer@ppu.edu
© 2026 The Authors. Published by University Malaysia Pahang Al-Sultan Abdullah Press. This is an open access article under the CC BY-NC 4.0 license

s, which is a significant gain, but the electrical consumption increased as well as the system complexity due to matching the fast electrical motor with the compressor shaft; in addition, the engine considered was a throttled SI engine. Other methods for increasing manifold pressure have been considered in the literature; e-compressors and e-turbos were studied by Yadla et al. [6] for throttled SI engines to compare vehicle performance based on different drive cycles.

However, several published results for compression-ignition engines show significant improvements in transient response; the automotive industry is heading toward hybrid powertrains with gasoline engines designed for lean-mixture operation. Bárdos and Németh [7] considered the use of compressed air to boost compression ignition engines to improve NO_x and soot formation during transients. Lee and Choi [8] have studied the potential of using proactive control of intake manifold pressure in compression-ignition engines to improve low- and fast-speed acceleration. Their results indicated noticeable improvements in the combustion characteristics and in-cylinder pressure, as well as reduced turbo lag, based on the compressor exit and turbine inlet operating conditions. Saad and Mishra [9] also used 1.0 bar of pressurized air-boosting assistance to reduce the turbo lag: A faster acceleration of 1.0 s, rather than 2.0 s, was observed for a compression-ignition engine. Shi et al. [10] proposed a synergistic framework for the transient response of electrified turbocharging systems based on a thermodynamic model. Their findings provide a theoretical basis for designing real-time, energy-efficient control strategies for next-generation zero-carbon powertrain systems. Vitek et al. [11] compared engine performance between a classical turbocharger and electrically assisted boosting, such as an e-turbo and an e-booster. They concluded that e-boosting significantly improved the engine transient response. Barman et al. [12] obtained similar results for diesel engine acceleration improvement. They assisted the turbocharger in reaching the required rpm threshold by using compressed air in the exhaust manifold to increase the intake boost pressure. This helps build rotational energy and reduce the turbo lag. Subramaniam and Wan Salim [13] compared electrical and conventional SI engine boosting in terms of fuel consumption.

The evaluation revealed potential improvements in the engine part-load and transient conditions, and a 2.6% increase in fuel consumption was observed at high engine speeds. The same authors [14] recently studied electric turbocharged engines to boost part-load during urban drive cycle conditions. Even with the control system complexity, the results proved better low-load performance than that of conventional turbocharged systems. Recently, Ozgur and Aydin [15] explored the effects of electrically assisted turbochargers on diesel engine performance. The results of the transient simulations showed notable improvements in engine torque at 1000 rpm and acceleration response times, with the turbo lag reduced by up to 53% under transient conditions. Similar results were published by Bao and Stobart [16], who compared three pneumatic hybrid boosting systems to reduce turbo lag, including intake and exhaust manifolds, using the GT-SUITE simulation code to evaluate the engine brake torque response and vehicle acceleration. Kołodziej and Mamala [17] considered vehicle acceleration based on the vehicle's overall characteristics related to performance, design, engine type, and inertia during acceleration. They used a short-term turbocharger system to solve the turbo lag problem by directly supplying compressed air to the turbine blade housing. The study showed improved vehicle acceleration in the medium- to high-speed range of 45–120 km/h. Similarly, Kindler et al. [18] tested compressed air delivery on the exhaust side of a turbocharger for a Volvo V70 2.0 Turbo vehicle. The aim is to improve the designs of older engines. The tested engine torque increased by up to 13% within the rotational speed range of 1700-2400 rpm. In another recent article, Xia et al. [19] considered improving the thermal efficiency of high-compression-ratio gasoline compression-ignition engines. They evaluated the injection control strategies under medium-to-high load conditions (BMEP of 1.1-1.8 MPa). However, they achieved a peak effective thermal efficiency of 48.4%. Engine performance under low load and speed conditions requires further development. Al-Muhsen et al. [20] studied emissions in a dual-fuel SI engine. The results revealed that increasing the DI from 10% to 100% and increasing the engine speed range from 3500 to 4000 rpm decreased the maximum cylinder pressure by 8.32% and increased the volumetric efficiency by 4.04% owing to the cooling effect. Ravaglioli et al. [21] presented an innovative control-oriented model to predict the maximum cylinder pressure of turbocharged gasoline direct-injection and naturally aspirated engines. They aimed to improve the sizing and calibration of electric hybrid powertrains using these engines. Arslan [22] investigated the SI engine efficiency and IMEP considering the improvements in the part-load volumetric efficiency. The focus was on the throttling losses during the exhaust and intake strokes of the engine. Improvements were achieved using combined methods, including VVT, VCR, and turbocharging. Wenz et al. [23] investigated the potential of lean-burn in combination with the volumetric efficiency variation technique to improve SI engine efficiency, which led to the typical outcome: increasing the charge specific heat ratio will affect engine thermal efficiency.

Most researchers have focused on mixture combustion and emissions at higher loads and speeds, as well as engine downsizing. However, the current SI engine technology trends are GTDI, lean-stratified mode for low-load and low-speed operating conditions, and lean-homogeneous mode for medium- to high-load and high-speed operating conditions. This trend is mainly due to two reasons: the first reason is that at medium- to high-loads and speeds, these engines operate close to their maximum efficiency range, and the improvement in their efficiency is quite small; while the second reason is that at high loads, the need is to benefit from all trapped oxygen to achieve the maximum power output. Thus, achieving a downsizing goal is limited by the stratification mode, and during high-load operation, GTDI engines tend to produce particulates in addition to other emissions due to locally rich mixture combustion. However, for the lean-stratified mode, it is possible to improve the transient thermal efficiency through air-boosting assistance without adding more fuel. Indeed, several leading automotive companies are pushing for an untargeted ICE 50% Brake Thermal Efficiency, which will favor the near-future scenario in which hybrid powertrains prevail and continue to do so in the foreseeable future, as explained by Conway et al. [24]. Furthermore, these insights help improve drivability performance under low- to medium-load and speed conditions, which are the main features of the Worldwide Harmonized Light Vehicles Test Cycle.

Accordingly, the main objective of this study was to increase the trapped mass at low speeds and loads when the turbocharger is not producing the required flow, which mitigates the engine turbo lag problem during vehicle transients. Therefore, the added value comes from the insights provided for improving the low-load and speed-transient performance. Of course, it can be adopted for higher load and speed operating conditions in the future as well. The adopted comprehensive model allows for the consideration of the vehicle's dynamic performance in terms of the turbocharger response and the changes in the intake manifold pressure. The model includes the gas-exchange processes of the engine, turbocharger, and vehicle dynamics. To improve the transient thermal efficiency of the GTDI engine, an intake manifold air injection technique was adopted, which requires minor and low-cost modifications to the engine. It helps with the immediate green transition to currently used technologies, especially those widely used in most low- and high-income countries. These insights will also enable the application of the same technique using hybrid powertrains and other fuels, including electro-fuels.

2. Materials and Methods

To investigate the main factors that affect the efficiency and related outputs of a GTDI SI engine, the specifications of commonly used engines were considered. In addition, a boosting assistance technique that injects pressurized air directly into the intake manifold after the turbocharger compressor is used, which ensures that the required faster engine response is achieved by delivering extra power during common low-speed vehicle-driving maneuvers. To carry out the required investigation and obtain insights into the potential for engine performance improvement, comprehensive modeling based on lumped-parameter and mean-value engine modeling was used to relate vehicle dynamics, gas exchange processes in the intake and exhaust manifolds, turbocharger dynamics, and engine power output. Finally, to demonstrate the effectiveness of the proposed technique, several simulations were performed using MATLAB codes. They cover the most common load and speed transients under urban driving conditions. The results are presented and thoroughly discussed, and then used in the conclusions and recommendations.

2.1 Modeling

In this study, a comprehensive model was used to relate vehicle dynamics to gas exchange processes in the intake and exhaust manifolds, turbocharger dynamics, and GTDI engine power output. The aim of this study was to demonstrate the effectiveness of air injection into the manifold during low-load transient operations and other loading conditions. The modeling is based mainly on the engine mean-value representation, which allows for an effective compromise between the precision in predicting the required variables and the model complexity. Modern intake and exhaust manifolds are distributed systems characterized by variable cross-sections and friction surfaces. In addition, disturbances initiated by moving pistons and valves travel back and forth along the manifolds, which affects the gas exchange processes. To account for such a complex physical behavior, which is beyond the scope of this study, parameters such as volumetric efficiency were estimated using a simplified model, and turbocharger flow rate as a function of pressure ratio and speed was based on empirical maps, while other parameters such as coefficients of discharge and those for vehicle road loads were adopted from well-recognized references such as Guzzella and Onder [25] and Heywood [26]. Figure 1 shows a schematic representation of the modeling, with the flow of the parameters highlighted.

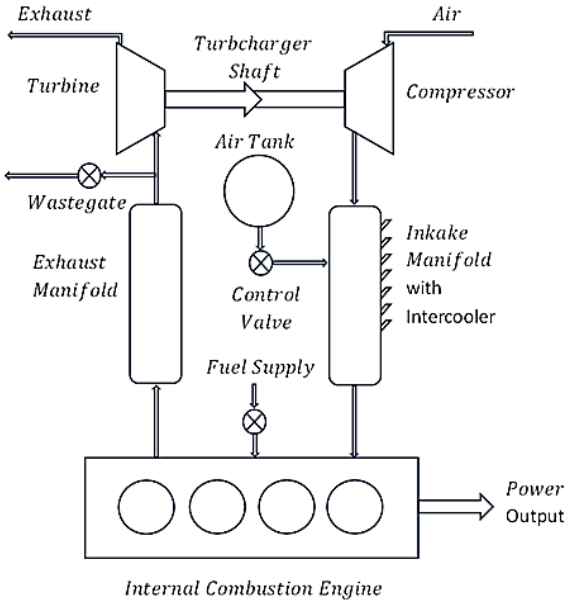


Figure 1. Schematic representation of the system modeling components

2.1.1 Intake manifold

To accurately represent the intake manifold dynamics, a lumped-parameter model was used to account for the intake manifold content dynamics. The model considers the manifold as a single capacity connected to the boosting system on

the input side and to the engine cylinders on the output side. This assumption allows the use of a single pressure and temperature to characterize the entire manifold capacity state. A closed volume around the intake manifold was used to estimate the rate of mass change inside the capacity and account for the mass flow to the engine cylinders. The conservation equations of mass and energy are applied, and the details of the assumptions and derivations are provided by Guzzella and Onder [25]. The resulting equations for the modelling are Eqs. (1–3):

$$\frac{dm_i}{dt} = \dot{m}_{co} + \dot{m}_a - \dot{m}_{cy} \tag{1}$$

$$\frac{dP_i}{dt} = \frac{\gamma_i R_i T_i}{V_i}\left(\dot{m}_{co} + \dot{m}_a - \dot{m}_{cy}\right) \tag{2}$$

$$\frac{dT_i}{dt} = \frac{R_i T_i}{c_{v,i} P_i V_i}\left(c_{p,co}\dot{m}_{co}T_{co} + c_{p,a}\dot{m}_a T_a - c_{p,i}\dot{m}_{cy}T_i - c_{p,i}\left(\dot{m}_{co} + \dot{m}_a - \dot{m}_{cy}\right)T_i - \dot{Q}_{ht}\right) \tag{3}$$

For the subsonic inflow from the compressor delivery side to the intake manifold, $(P_{co} - P_i) > 0$, Benson [27]:

$$\dot{m}_{co} = \rho_i C_d A_i \left\{ \frac{\frac{2\gamma_i R_i T_i}{\gamma_i - 1}\left[P_{cr}^{(\gamma_i - 1)/\gamma_i} - 1\right]}{\left[\frac{1}{\varphi^2} P_{cr}^{2/\gamma_i} - 1\right]} \right\}^{\frac{1}{2}} \tag{4}$$

$P_{cr} = P_{co}/P_i$ and $\varphi = A_i/A_{co} \approx 1$

For the outflow from the intake manifold to the engine cylinders:

$$\dot{m}_{cy} = \rho_i V_d \eta_v \frac{N_e}{n_r 60} = \frac{V_d \eta_v N_e}{n_r 60}\frac{P_i}{R_i T_i} \tag{5}$$

$\rho_i = P_i/(R_i T_i)$

where m_i is the air mass inside the intake manifold, $\dot{m}_{co}$ is the air mass flow rate from the compressor output side into the intake manifold, $\dot{m}_a$ is the air mass flow rate from the air injection system into the intake manifold, $\dot{m}_{cy}$ is the air mass outflow rate from the intake manifold into the engine cylinders, P_i and T_i are the intake manifold contents pressure and temperature, respectively, $\dot{Q}_{ht}$ is the heat transfer between the walls and gas within the intake manifold (using eq. (7)), C_d is the intake pipe coefficient of discharge, A_i is the intake pipe cross-section, A_{co} is the compressor delivery pipe cross-section, P_o and T_o are the atmospheric pressure and temperature, respectively, R_i is the intake flow gas constant, γ_i is the intake flow specific heat ratio, P_{co} is the compressor delivery-side pressure (Turbocharger characteristics that are used in this study are assumed to be within the turbocharger stable operating range, where the map for speed and efficiency are related to pressure ratio against mass flow, Heywood [26] and Benson [27]; more details on the adopted characteristics are given in Section 3.4). V_d is the engine displacement volume, N_e is the engine speed (rpm), η_v is the engine volumetric efficiency, using the simplified Eq. (6), n_r is the number of revolutions of the crankshaft per cycle ($n_r = 2$ for four-stroke cycles), and ρ_i is the manifold content density.

For estimating the volumetric efficiency, the exhaust gases are assumed to be perfect gases with constant γ_e and isentropic processes. Then, using the pressure-dependent part of the volumetric efficiency modeling by Guzzella and Onder [25], which mainly describes the effects caused by the trapped exhaust gas for an ideal cycle, the volumetric efficiency can be approximated as follows:

$$\eta_v = \frac{V_{ch} + V_d}{V_d} - \left(\frac{P_e}{P_i}\right)^{\gamma_e}\frac{V_{ch}}{V_d} \tag{6}$$

where P_e is the pressure at the engine's exhaust side, assumed constant, and V_{ch} is the combustion chamber volume.

For heat transfer between the walls and air within the intake and exhaust manifolds, including the intercooler, the following simplified model was adopted. Fortunately, the mean value modeling assumes continuous flow, which is sufficiently accurate.

$$\dot{Q}_{ht} = \left(\frac{P_i V_i}{R_i T_i}\right)\left(\frac{2 f c_p |\bar{u}_i|}{D}\right)(T_w - T_i) \tag{7}$$

where R_i is the gas constant, f is the gas-surface friction coefficient, c_p is the gas pressure specific heat constant, D is the mean duct diameter, $\bar{u}_i$ is the mean flow speed, T_w is the manifold wall mean temperature, and T_i is the mean gas temperature.

For air injection to boost the intake manifold contents, the application of energy conservation for isentropic subsonic flow from a reservoir through a restriction or valve, as suggested by Guzzella and Onder [25] and others, yields

$$\dot{m}_a = \frac{C_d A_a P_a}{\sqrt{R_a T_a}} \left(\frac{P_i}{P_a}\right)^{1/\gamma_a} \left[\frac{2\gamma_a}{\gamma_a - 1}\left(1 - \left(\frac{P_i}{P_a}\right)^{\left(\frac{\gamma_a - 1}{\gamma_a}\right)}\right)\right]^{1/2} \tag{8}$$

where $\dot{m}_a$ is the air mass flow rate from the boosting air reservoir, C_d is the valve coefficient of discharge, A_a is the boosting valve cross-section, P_a and T_a are the boosting air reservoir pressure and temperature, respectively, R_a is the air gas constant, γ_a is the air specific heat ratio, P_i is the intake manifold-side pressure.

2.1.2 Exhaust manifold

To model the exhaust manifold dynamics, the conservation equations of mass and energy are applied as those for the intake manifold; the assumptions and derivations are also similar. Therefore, the resulting equations for the modelling are Eqs. (9–12):

$$\frac{dm_e}{dt} = \dot{m}_{cy,o} - \dot{m}_{tr} - \dot{m}_{wg} \tag{9}$$

$$\dot{m}_{cy,o}(t - \tau_c) = \dot{m}_{cy}(t)\left(1 + \frac{1}{\phi}\right) \tag{10}$$

$$\frac{dP_e}{dt} = \frac{\gamma_e R_e T_e}{V_e}\left(\dot{m}_{cy,o} - \dot{m}_{tr} - \dot{m}_{wg}\right) \tag{11}$$

$$\frac{dT_e}{dt} = \frac{R_e T_e}{c_{v,e} P_e V_e}\left(c_{p,c}\dot{m}_{cy,o}T_{c,o} - c_{p,e}\dot{m}_{tr}T_e - c_{p,e}\dot{m}_{wg}T_e - c_{p,e}\left(\dot{m}_{cy,o} - \dot{m}_{tr} - \dot{m}_{wg}\right)T_e - \dot{Q}_{ht}\right) \tag{12}$$

For the exhaust flow to the turbocharger pipe, the application of energy conservation for isentropic subsonic flow through a restriction or valve from a reservoir is similar to the case of Eq. (8), gives:

$$\dot{m}_{tr} = \frac{C_d A_e P_e}{\sqrt{R_e T_e}} \left(\frac{P_{tr}}{P_e}\right)^{1/\gamma_e} \left[\frac{2\gamma_e}{\gamma_e - 1}\left(1 - \left(\frac{P_{tr}}{P_e}\right)^{\left(\frac{\gamma_e - 1}{\gamma_e}\right)}\right)\right]^{1/2} \tag{13}$$

where m_e is the air mass inside the exhaust manifold, $\dot{m}_{cy,o}$ is the gas flow rate from the engine cylinders into the exhaust manifold, $\dot{m}_{tr}$ is the exhaust flow into the turbocharger pipe, $\dot{m}_{wg}$ is the gas flow rate through the wastegate (bypassing the turbocharger), P_e and T_e are the exhaust manifold contents pressure and temperature, respectively, $\dot{Q}_{ht}$ is the heat transfer between the walls and gas within the exhaust manifold (using Eq. (7)), C_d is the intake pipe coefficient of discharge, A_e is the exhaust pipe cross-section, P_{tr} is the turbocharger delivery pipe pressure (depends on the turbocharger characteristics map), R_e is the exhaust gas flow constant, γ_e is the exhaust flow specific heat ratio, τ_c is the cycle delay time between filling and emptying engine cylinders, and ϕ is the air-fuel ratio.

2.1.3 Engine cylinder

The in-cylinder processes of a real internal combustion engine are inherently irreversible. This implies, based on the second law of thermodynamics, that the entropy is not constant within the engine cylinder due to dissipative effects and finite gradients. Therefore, true isentropic conditions cannot exist in a functioning engine. Entropy variation in the engine cylinder occurs owing to irreversibilities from flow through the valves, temperature gradients, heat transfer, and friction. Therefore, it needs to be considered with sufficient accuracy for the required modeling purposes. To account for cylinder pressure changes, it is assumed that pressure and temperature are uniform at any instant, and the first law of thermodynamics is applied to the cylinder volume as an open system. The irreversibilities resulting from heat transfer and friction were included using the empirical relations suggested by Heywood [26] and Benson [27]. The adopted relation uses the mean values of the piston speed and cylinder content temperature. The solution it offers is acceptable for engine control purposes. Assuming the fuel is fully evaporated, where P_c, T_c, V_c, m_c and u_c represents the pressure, temperature, volume, mass, and specific internal energy of the in-cylinder gas, respectively, and the cylinder pressure is given by

$$\frac{dP_c}{dt} = \frac{1}{V_c}\left\{\gamma_i R_i T_i \dot{m}_{cy} - \gamma_e R_e T_e \dot{m}_{cy,o} - \gamma_e P_c \frac{dV_c}{dt} + (\gamma_e - 1)\frac{dQ_{cy}}{dt}\right\} \tag{14}$$

Eq. (14) is applied to each cylinder of a multi-cylinder engine as a function of the cylinder volume change, in addition to the intake and exhaust valve opening and closing times. In addition, taking into account the heat release start and end were considered based on the crankshaft angle, and the Wiebe function was used to estimate the in-cylinder heat release. The (dQ_{cy}/dt) represents the heat transfer and heat release components in the cylinder:

$$\frac{dQ_{cy}}{dt} = \frac{dQ_{cy,ht}}{dt} + \frac{dQ_{cy,hr}}{dt} \tag{15}$$

The component $Q_{cy,ht}$ represents the heat transfer between the gas and cylinder walls and is given by

$$\frac{dQ_{cy,ht}}{dt} = \frac{\beta R_n^{\sigma}}{D_c} k_q A_w (T_w - T_c) \tag{16}$$

$R_n = \rho_c D_c \bar{u}_p / \mu_{air}$ and $\mu_{air} = 3.3 \times 10^{-7} \times T_c{}^{0.7}$

where β and σ are constants, A_w is the exposed surface area of the cylinder walls plus piston area and cylinder head area, D_c is the cylinder bore, T_w is the mean wall temperature, T_c is the mean gas temperature, R_n is the Reynolds number, ρ_c is the gas density, μ_{air} is the gas viscosity, $\bar{u}_p$ is the average piston velocity, k_q is the conductivity (at Prandtl number $Pr = 0.7$) = $C_p \mu / Pr$, C_p is the specific heat of the gas at constant pressure. $\sigma = 0.7$ as recommended in the relevant literature, Benson [27], and the value of β varies from 0.38 to 0.8, depending on the engine design, and increases with the intensity of charge motion. While μ_{air} is given in $kg/m.s$ and the temperature is in Kelvin. The temperature of the combustion chamber walls varies depending on the surface; the cylinder walls are approximately 180 °C to protect the lubricating oil film, the intake valve head surface temperatures are 150–250 °C depending on the operating conditions, and the piston topside can reach much higher temperatures, as in the cylinder head where the exhaust valves are located, as given by Heywood [26]. An average temperature is sufficiently accurate for estimating the heat flux. The component $Q_{cy,hr}$ represents the heat release due to the combustion of the mixture in the cylinder and is given by

$$Q_{cy,hr} = \left(\frac{Q_{LHV} m_{cy}}{\phi}\right) x_b \tag{17.a}$$

$$x_b = 1 - exp\left(-a\left(\frac{\theta_c - \theta_s}{\theta_d}\right)^n\right) \tag{17.b}$$

where Q_{LHV} is the fuel lower heating value, m_{cy} cylinder trapped air mass, x_b is the Wiebe function for fuel mass fraction burned in relation to crankshaft angle (varies from $x_b = 0$ to $x_b = 1$), θ_c is the crankshaft angle, θ_s is the start of combustion, θ_d is the combustion duration, and a and n are adjustable parameters; typical values are $a = 5$ and $n = 3$, Ferguson and Kirkpatrick [28]. The cylinder volume and rate of change of volume are given by

$$V_c = \frac{A_c S_t}{2}\left\{1 + \varepsilon - \sqrt{\varepsilon^2 - sin^2\,\theta_c} - cos\,\theta_c + \frac{2}{r_c - 1}\right\} \tag{18.a}$$

$$\frac{dV_c}{dt} = \frac{\omega_e A_c S_t}{2}\left\{sin\,\theta_c + \frac{1}{2}\left(\frac{sin\,2\,\theta_c}{\sqrt{\epsilon^2 - sin^2\,\theta_c}}\right)\right\} \tag{18.b}$$

where A_c is the cylinder cross-sectional area, S_t is the stroke, ε is the ratio of the connecting rod length to the crankshaft radius, θ_c is the crankshaft angle, r_c is the nominal compression ratio, ω_e is the engine speed rad/s.

To account for the temperature changes in the engine cylinder contents, the state equation can be applied, given that the in-cylinder gas pressure, mass, and volume are known. The mass of the cylinder contents can also be estimated by applying the continuity equation to the engine cylinder.

2.1.4 Turbocharger

The function of the turbocharger is to compress fresh air before the engine cylinders using a centrifugal compressor coupled to an exhaust-gas-driven turbine. This increases the power output for the same displacement volume. A wastegate is generally incorporated to bypass the turbine inlet, which helps avoid over-boosting of the engine cylinders. Given that at low engine speeds and loads, the turbocharger has little impact on the engine's operational performance, this has led to the use of small-size turbochargers to achieve a rapid rise in power output at low engine speeds or large-size turbochargers to increase the air mass per cycle for better thermal efficiency through the mid-speed range. Many leading automotive companies, such as Volkswagen, Mitsubishi, and Peugeot, have considered using variable-geometry turbochargers to achieve high-performance engines or optimize the Miller cycle and transient performance. This allows for achieving the required compromise between the various operating conditions. However, in all cases, the turbo lag during transient conditions affected the engine response. Consequently, it affects the vehicle drivability performance. This contribution addresses this issue by considering the direct injection of pressurized air into the intake manifold, which could result in a faster engine boost during transient conditions, particularly at low speeds and loads, where the turbo-lag effect is evident.

But, given that the turbocharger design is based on matching turbine and compressor characteristics based on air and exhaust flow along with pressure ratios and engine speed to avoid model complexity, the estimation of air-mass flow through the compressor will be based on typical maps; they relate corrected speed $(N_{tr}(rpm)/\sqrt{T_o(°K)})$, compressor efficiency $\eta_{co,is}$ and pressure ratio P_{co}/P_o against corrected mass flow $\dot{m}_{co}(kg/s)\sqrt{T_o(°K)}/P_o$. For this contribution, typical values for stable turbocharger operational characteristics were used, Heywood [26] and Benson [27]: Pressure ratio range is from 1.5 to 2.5, corrected mass flow range is from 2.0 to 4.5, compressor efficiency range is from 0.72 to 0.75, and corrected speed range is from 4000 to 6000. Thus, the maximum intake manifold pressure was set as a threshold to avoid over-boosting conditions or approaching the compressor surge limit. To account for the turbocharger dynamics, the following equation was adopted from the study by Moraal and Kolmanovsky [29]:

$$J_{tr}\frac{d\omega_{tr}}{dt}=\frac{1}{\omega_{tr}}\left(\dot{W}_{tr}-\frac{\dot{W}_{co}}{\eta_m}\right) \tag{19}$$

where J_{tr} is the turbocharger total rotational inertia, N_{tr} is the turbocharger shaft rotational speed, ω_{tr} is the turbocharger shaft angular speed, $\dot{W}_{tr}$ is the turbine output power, $\dot{W}_{co}$ is the power required to drive the compressor, η_m is the combined turbocharger mechanical efficiency, which is primarily caused by bearing friction losses. The power delivered by the turbine is expressed as

$$\dot{W}_{tr}=\dot{m}_{tr}c_{p,e}T_e\eta_{TTS}\left(1-\left(\frac{P_{tr}}{P_e}\right)^{\left(\frac{\gamma_e-1}{\gamma_e}\right)}\right) \tag{20.a}$$

$$\frac{T_{tr}}{T_e}=\left(\frac{P_{tr}}{P_e}\right)^{\left(\frac{\gamma_e-1}{\gamma_e}\right)} \tag{20.b}$$

where the subscript e denotes exhaust gas properties, η_{TTS} is the total-to-static turbine efficiency, P_{tr} and T_{tr} are the pressure and temperature at the turbine exit, respectively. The power required to drive the compressor is expressed as

$$\dot{W}_{co}=\frac{\dot{m}_{co}c_{p,a}T_o}{\eta_{CTS}}\left(1-\left(\frac{P_{co}}{P_o}\right)^{\left(\frac{\gamma_a-1}{\gamma_a}\right)}\right) \tag{21.a}$$

$$\frac{T_{co}}{T_o}=\left(\frac{P_{co}}{P_o}\right)^{\left(\frac{\gamma_a-1}{\gamma_a}\right)} \tag{21.b}$$

where the subscript a denotes intake air properties, η_{CTS} is the total-to-static compressor efficiency, P_{co} and T_{co} and are the pressure and temperature of the compressor delivery side, respectively.

2.1.5 Vehicle Dynamics

Road loads and powertrain dynamics were included in the model, as given by Gillespie [30]. Then, after rearrangement, the following equations can be obtained to account for vehicle longitudinal dynamics; the following equations apply:

$$m_v\dot{v}=F_{xf}+F_{xr}-R_x \tag{22.a}$$

$$R_x=R_a+R_r+R_g \tag{22.b}$$

$$R_a=\frac{\rho}{2}C_DA_Fv_r^2 \tag{22.c}$$

$$R_r=\mu_f m_v g \tag{22.d}$$

$$R_g=m_v g\,sin\,\theta \tag{22.e}$$

where m_v is the vehicle mass, v is the vehicle speed, F_{xf} and F_{xr} are the front and rear drive/brake force respectively, R_x is the road loads that include three components: R_a is the air drag, R_r is the rolling resistance, and R_g is the road surface inclination load, ρ is the air density, C_D is the drag coefficient, A_F is the vehicle projected frontal area, v_r is the relative velocity between the vehicle and the wind, μ_f is the rolling resistance coefficient, and θ is the road surface inclination. To account for the longitudinal velocity changes, the following equations apply:

$$\dot{v}=\frac{1}{M_n}\left(\frac{\eta_t\zeta_t}{R_w}T_e-R_x\right) \tag{23}$$

where $M_n=M_Fm_v$ is the effective vehicle mass, including the powertrain inertia and gear ratio. M_F is the vehicle mass factor, ζ_t is the powertrain total gear ratio, η_t is the powertrain total efficiency, R_x is the driving wheel radius, T_e is the engine torque, either in driving or braking. For passenger cars, the mass factor is given by $M_F=1.04+0.0025{\zeta_t}^2$ and the vehicle speed is given by $v=\omega_eR_w(1-i)/\zeta_t$, where ω_e is the engine speed, R_w is the wheel effective radius, and i is the tire slip, which is negligible for this contribution, Gillespie [30].

3. Results and Discussion

The considered cases mainly cover transients during some typical low and medium drive ranges to provide insights into the effect of various specific parameters along with the air boosting assistance to simulate real driving conditions, including engine speed changes, gear ratio changes, road loads, intake manifold pressure changes, air-fuel ratio changes, turbocharger operating parameter changes, and different combinations of parameters. The simulation results were obtained and grouped into five cases, with special attention to common extra-urban driving maneuvers regarding speed and road conditions. The simulations were conducted for real vehicle maneuvers, including variable-speed conditions, which also accounted for all longitudinal dynamics. The results were also compared with those of the case without air-boosting assistance to highlight the effects. The results included the engine torque, speed, IMEP, intake manifold pressure,

in-cylinder pressure, and vehicle speed. Table 1 lists all the vehicle specifications and engine parameters used in this study.

Table 1. Vehicle specifications

Parameter	Value	Parameter	Value
Sprung Mass	2450 kg	1st Gear Ratio	5.250:1
Unsprung Mass	55 kg	2nd Gear Ratio	3.360:1
Mass Distribution, %F/R	55/45	3rd Gear Ratio	2.172:1
Wheelbase	2.68 m	4th Gear Ratio	1.720:1
Rear Track	1.52 m	5th Gear Ratio	1.316:1
Front Area	2.22 m^2	6th Gear Ratio	1.000:1
Air Drag Coefficient	0.24	7th Gear Ratio	0.822:1
Centre of Gravity Height	0.515 m	8th Gear Ratio	0.640:1
Wind Force Centre Height	0.5 m	R Gear Ratio	3.712:1
Rolling Coefficient	0.01	Final Drive Ratio	2.813:1
Tires Radius	0.3 m	Cam Periods	268°
Road Friction Coefficient	0.8	Inlet Valve Open	34° BTDC
Displacement Volume	1998 cc	Inlet Valve Close	54° ABDC
Number of Cylinders	4	Exhaust Valve Open	74° BBDC
Stroke/Bore	94.6/82.0 mm	Exhaust Valve Close	14° ATDC
Compression Ratio	11:1	Throttle Inlet Diameter	70 mm
Maximum Torque	250 Nm	Intake Manifold Volume	2800 cc

3.1 Effects of Boosting Assistance Pressure

Vehicle acceleration depends directly on the engine-produced torque and, consequently, on the in-cylinder pressure, which depends on the trapped mixture mass and strength. GTDI engines are designed to increase the trapped mass and reduce the strength to achieve leaner combustion and higher thermal efficiency operating conditions. The relevant literature shows that supplying boosted air increases the net IMEP and torque of the engine. However, the spark timing still needs to be adapted because the combustion of a leaner mixture is slower. Consequently, the exhaust gas temperature and enthalpy increase at higher engine speeds, thereby increasing the force on the turbine blades. Thus, during short-term accelerations, this helps drive the turbocharger faster owing to the stronger exhaust flow, which consequently increases the boost pressure. To achieve maximum brake torque during low-speed transients, it is sufficiently accurate to assume that the variation in combustion duration is very small and thus negligible, which allows the combustion timing to be related linearly to the crank angle and engine speed. In addition, the considered range is generally characterized by a relatively small effect of the turbocharger on the cylinder charge, whereas the major effect is due to the air-boosting assistance. For this study, the maximum intake manifold pressure could be in the range of 1.8-2.0 bar for these engines with a maximum BMEP of 20-25 bar, as given by Heywood [26]. Figure 2 presents the effects of boosting pressure on engine output and vehicle acceleration at low speed and air injection into the intake manifold at boosting pressures of 1.75, 2.0, and 2.25 bar. In addition, the relative air-fuel ratio was constant, and the transmission was in the first gear. The per-cylinder IMEP increased from 11.1 to 18.2 bar, and the engine torque increased from 44 to 72.4 Nm, which is a significant improvement in response to the increase in manifold pressure. In Case A (1.75 bar), the cylinder air mass increased to 4.0 g at the start of the air injection and then decreased to 2.7 g owing to the engine acceleration. In Case B (2.0 bar), the cylinder air mass increased to 4.9 g and then decreased to 3.0 g. In Case C (2.25 bar), the cylinder air mass increased to 5.7 g and then decreased to 3.4 g. Typically, as the engine accelerates, less mass is trapped in the cylinder if the upstream conditions are constant. Thus, to maintain the same mass trapped during acceleration and a higher transient thermal efficiency, it is necessary to use a variable-flow orifice or increase the air injection pressure. Also, the exhaust specific heat ratio is higher than that of typical engines ($\gamma_e = 1.3484$), which is useful for engine downsizing and improving vehicle drivability.

3.2 Effects of Boosting Assistance with Air-Fuel Ratio

GTDI engines are operated in a homogeneous lean mode, with a mixture relative air-fuel ratio in the $\lambda = 1.0 – 1.3$ range, where the engine operates under medium- to high-load conditions, close to the high-efficiency range. However, the design of these engines is more about improving thermal efficiency during the low- to medium-operating range, where the stratified charge mode using a leaner mixture with an AFR range of $\lambda = 1.6 – 3.4$ helps to improve thermal efficiency, benefiting from the increase in in-cylinder air mass due to unthrottled operation, which fully agrees with the results outlined by Duan *et al.* [31]. In addition, Ferrari and Pizzo [32] discussed the decrease in exhaust energy and wall heat transfer as the relative air-fuel ratio increased, which positively affected the engine net output. Figure 3 presents the effect of boosting assistance on the engine output and vehicle acceleration response owing to the air-fuel ratio variation by air injection into the intake manifold while keeping the fuel flow constant.

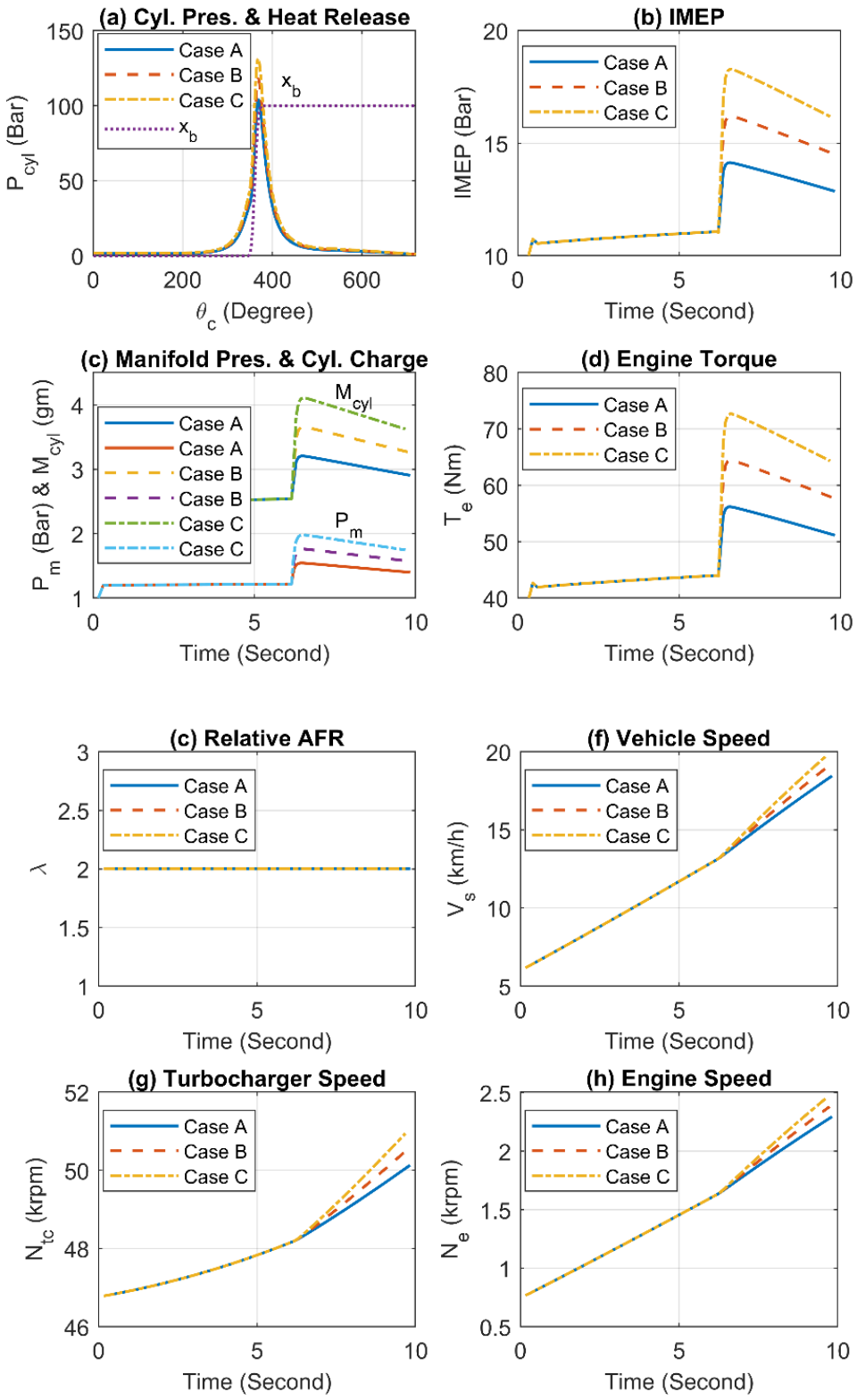


Figure 2. Effect of boosting assistance pressure on vehicle acceleration using the test's initial values: $N_e = 750\ rpm$, $\lambda = 2.0$, and 1st Gear Ratio. Case A: Boosting assistance $P_a = 1.75\ bar$; Case B: Boosting assistance $P_a = 2.0\ bar$; Case C: Boosting assistance $P_a = 2.25\ bar$

Test conditions start with a low speed of $N_e = 750$ rpm, $\lambda = 2.0$, air injection pressure $P_a = 2.25$ bar and 1st gear ratio. This shows that the IMEP and torque increase when the manifold pressure increases, while allowing the vehicle to maintain acceleration without increasing the fuel quantity. The boosting air mass for Case A is 0.0 gm and for Case B started at 5.7 gm, then decreased to 3.6 gm, while for Case C started at 5.7 gm then decreased to 3.4 gm due to engine acceleration, and the exhaust specific heat ratio is $\gamma_e = 1.3484$, which is similar to that in the previous section.

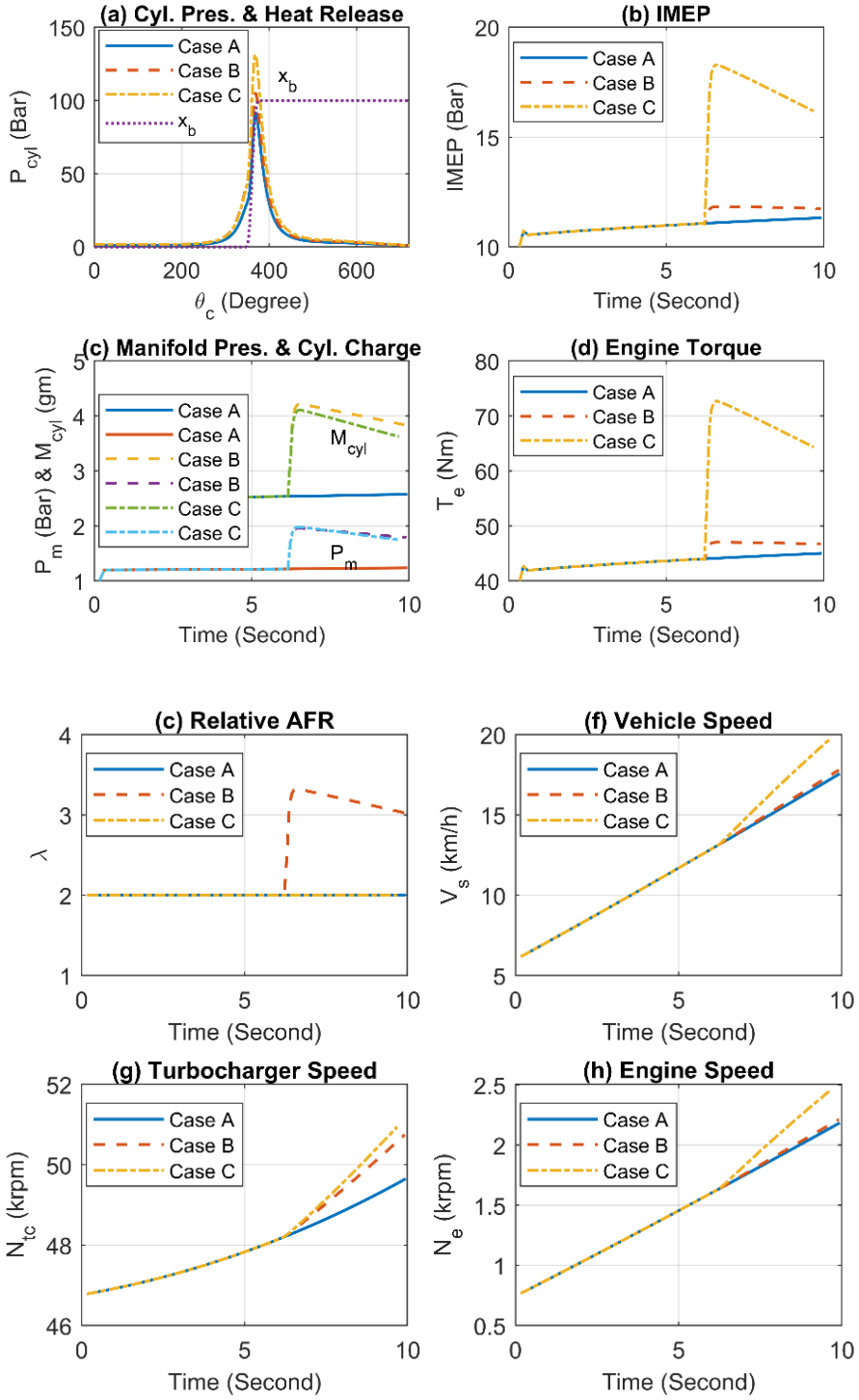


Figure 3. Effect of air-fuel ratio on vehicle acceleration using initial values: $N_e = 750\ rpm$, $\lambda = 2.0$, $P_a = 2.25\ bar$ and 1st Gear Ratio. Case A: Without boosting assistance and constant AFR; Case B: with boosting assistance and constant AFR; Case C: with boosting assistance and variable AFR

3.3 Effects of Powertrain Dynamics

The response of the powertrain dynamics is highly dependent on the vehicle speed at a given gear ratio, as confirmed in many studies. Aydin and Kirmaz [33] investigated the wheel power and lambda values at different gear ratios and speeds to establish their relationship with emission variations, emphasizing their importance. In fact, the gear ratio becomes more influential on the vehicle acceleration response at higher speeds, which emphasizes that better drivability could be achieved using the first gear ratio together with boosting assistance to minimize the powertrain's negative effect, thus improving drivability and allowing for engine downsizing. Figure 4 presents a case comparison to account for the powertrain dynamics: 1st, 2nd, and 3rd, which are the ratios for the low to medium range. The results show a positive effect on powertrain dynamics at the first gear ratio: a steeper acceleration response slope with faster engine and turbocharger acceleration. The results also confirmed the inverse relationship between the gear ratio and acceleration

gradient owing to the boosting pressure. The simulation starting conditions are engine speed of $N_e = 1500$ rpm and air injection pressure $P_a = 2.0$ bar at constant relative AFR $\lambda = 2.0$. The results per cylinder showed that the IMEP increased from 11 to 16.5 bar, and the torque increased from 44 to 73 Nm owing to the increased manifold pressure. The boosting air mass for Case A started at 4.1 gm, then decreased to 3.0 gm, and Case B started at 4.6 gm, then decreased to 3.2 gm, while Case C started at 4.9 gm, then decreased to 3.4 gm due to engine acceleration, and the exhaust specific heat ratio is $\gamma_e = 1.3484$.

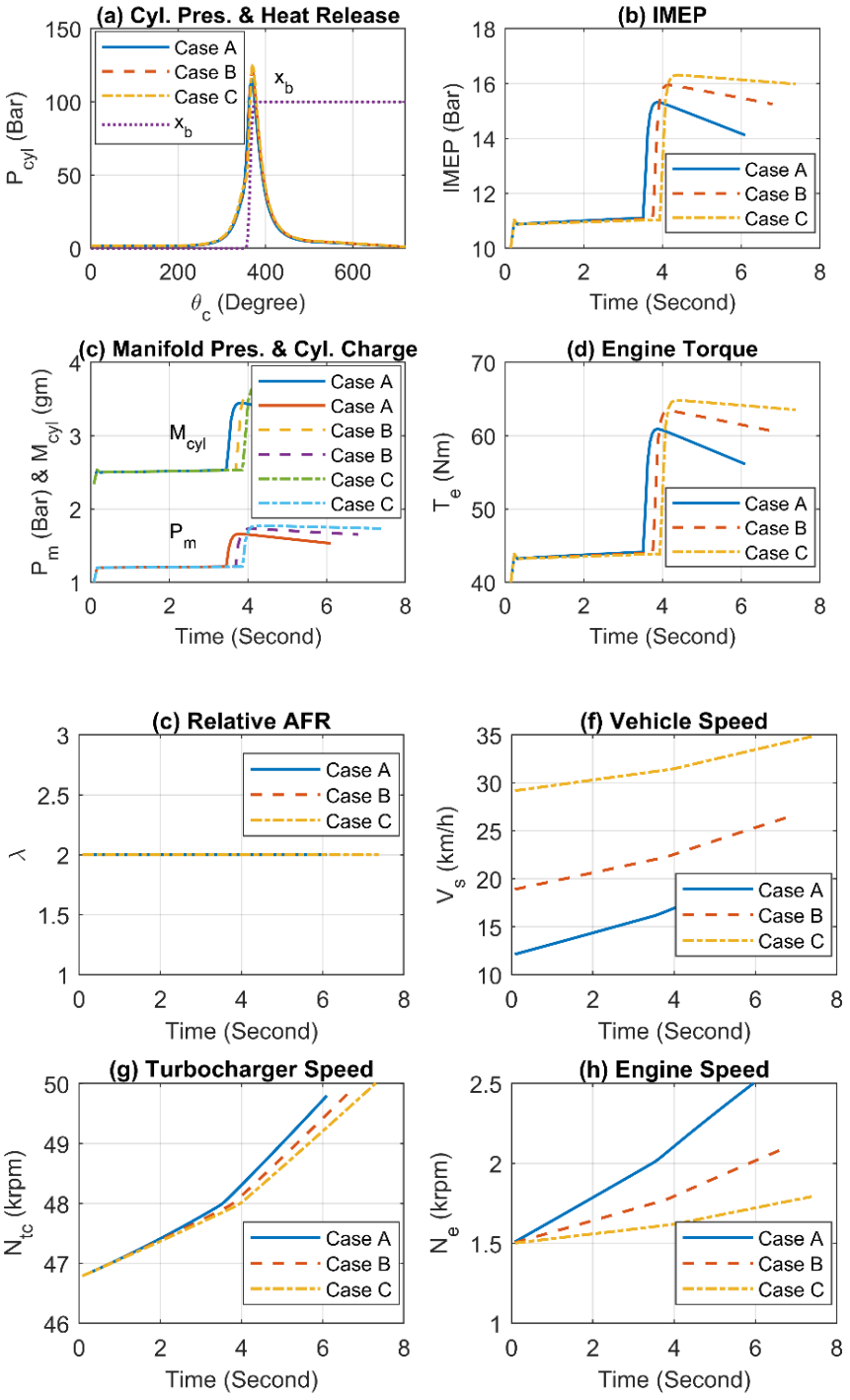


Figure 4. Effect of powertrain dynamics on vehicle acceleration using the test's initial values: $P_a = 2.0\ bar$, $\lambda = 2.0$, and $N_e = 1500\ rpm$. Case A: Boosting assistance at 1st Gear Ratio; Case B: Boosting assistance at 2nd Gear Ratio; Case C: Boosting assistance at 3rd Gear Ratio

3.4 Effects of Road Load Dynamics

Vehicle response to air drag, rolling resistance, and road inclination is also reflected in the adopted modeling. Air drag depends directly on vehicle speed, whereas rolling resistance and road inclination do not. Accordingly, the road loads, which are accounted for using Eq. (22) become more influential on vehicle acceleration at higher vehicle speeds. Thus, the outcome that for better drivability, it is better to use first gear ratios along with boosting assistance is emphasized.

Figure 5 presents a comparison between three different engine speeds at a specific gear ratio to account for road load dynamics: $N_e = 1000,\ 2000, and\ 3000$ rpm; low to medium range. The results show a clear positive effect of boosting assistance on the vehicle acceleration response slope, with faster engine and turbocharger accelerations at lower engine speeds. The results also confirmed the direct inverse relationship between the vehicle longitudinal speed and acceleration gradient owing to the boosting assistance pressure. The considered effects starting conditions are air injection pressure $P_a = 2.0$ bar at constant relative air-fuel ratio $\lambda = 2.0$ and 3rd gear ratios. In addition, as in the previous sections, there are obvious improvements in the IMEP and engine torque for increasing manifold pressure at lower speeds. The boosting air mass for Case A started at 6.2 gm, then decreased to 3.6 gm; Case B started at 3.9 gm, then decreased to 3.1 gm; while Case C started at 2.8 gm, then decreased to 2.6 gm due to acceleration, and the exhaust specific heat ratio is $\gamma_e = 1.3484$.

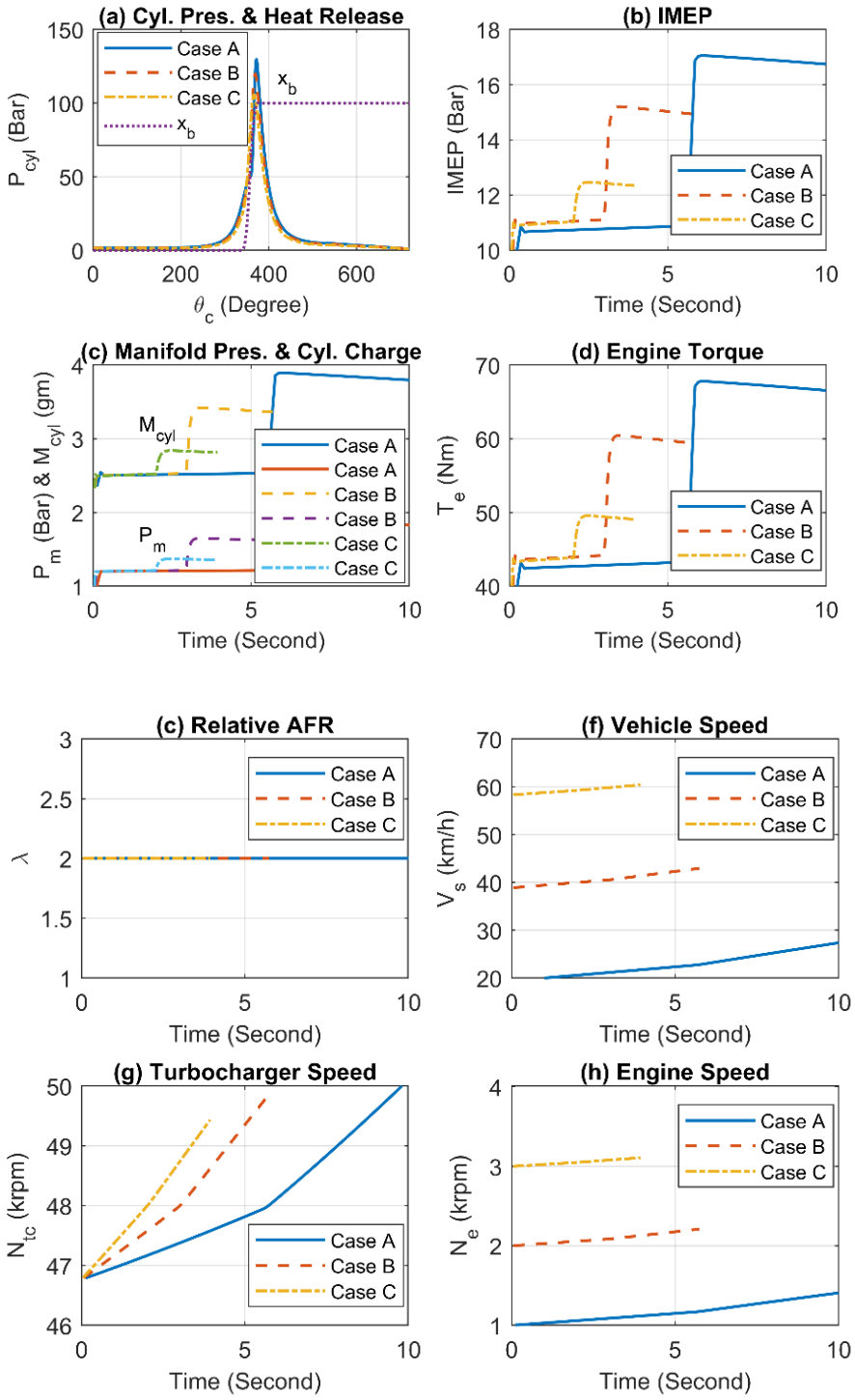


Figure 5. Effect of road load dynamics on vehicle acceleration using the test's initial values: $P_a = 2.0\ bar$, $\lambda = 2.0$, and 3rd Gear Ratio. Case A: Boosting assistance at $N_e = 1000\ rpm$; Case B: Boosting assistance at $N_e = 2000\ rpm$; Case C: Boosting assistance at $N_e = 3000\ rpm$.

3.5 Effects of Combined Factors

The results for the vehicle acceleration response owing to the combined factor effects are shown in Figure 6. Road loads and powertrain dynamics that reflect real driving maneuvers were combined with air-fuel ratio variation by allowing air injection in the intake manifold while keeping the fuel flow constant. Using gear ratio changes at a constant engine speed, the results indicate that the vehicle has improved performance owing to boosting assistance even with less fuel flow, which is highlighted by the increase in the relative air-fuel ratio when compared to the pre-assistance phase, emphasizing better drivability performance using first gear ratios along with boosting assistance with faster engine and turbocharger acceleration. The comparison includes three gear ratios: 1st, 2nd, and 3rd gear ratios in the low to medium range. The results are based on air injection pressure $P_a = 2.0$ bar and engine speed of $N_e = 1500$ rpm with an initial value of relative air-fuel ratio of $\lambda = 2.0$. This shows that even without additional fuel, the IMEP and engine torque are maintained by increasing the manifold pressure. Case A: The boosting air mass varies between 4.1-3.1 gm and exhaust specific heat ratio varies between 1.3484-1.3623; Case B: The boosting air mass varies between 4.6-3.3 gm and exhaust specific heat ratio varies between 1.3484-1.3639; Case C: The boosting air mass varies between 4.9-3.5 gm and exhaust specific heat ratio varies between 1.3484-1.3648, where the γ_e variation was due to acceleration.

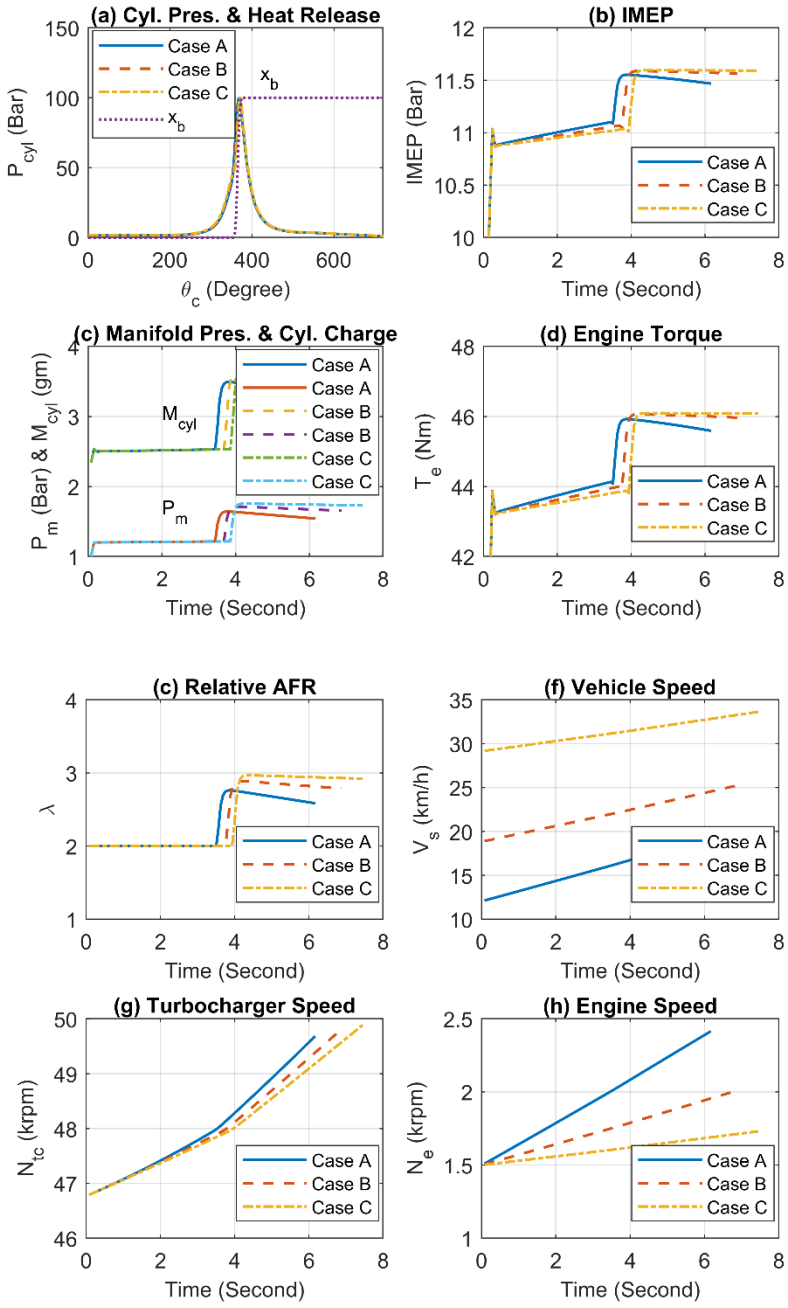


Figure 6. Effect of combined factors on vehicle acceleration using the test's initial values: $P_a = 2.0\ bar$, $\lambda = 2.0$, and $N_e = 1500\ rpm$. Case A: Boosting assistance at 1st Gear Ratio; Case B: Boosting assistance at 2nd Gear Ratio; Case C: Boosting assistance at 3rd Gear Ratio.

3.6 Results Summary and Comparison

The obtained results for the vehicle acceleration response owing to the combined effects of the factors are listed in Table 2, where the variation in the main performance parameters owing to the effects of boosting pressure variation, effects of boosting assistance with air-fuel ratio variation, effects of powertrain dynamics owing to gear ratio variation, effects of road load dynamics owing to engine speed variation, and effects of combined factors are shown. The results in all cases showed similar improvements in IMEP and torque, particularly owing to the increased manifold pressure at lower speeds. The boosting air mass starts at a given value, then decreases to a lower value owing to engine acceleration but maintains sufficient boosting assistance for the transient maneuver time. The results show a noticeable improvement in the thermal efficiency and transient performance.

To appreciate the results, the basic relations for the main parameters are presented in this section. The work output per cylinder of a four-stroke engine is given by $W_c = \eta_c \oint P_c dv_c$, then the power will be given by $Power = W_c/\tau_c$, the indicated mean effective pressure will be given by $imep = W_c/V_d$, the torque will be given by $T_e = Power/\omega_e$, and the engine thermal efficiency is given by $\eta_{th} = W_c/(LHV \cdot m_{cy}/AFR)$, where P_c is the cylinder pressure, v_c is the cylinder volume, η_c is combustion efficiency - assumed to equal one, τ_c is the cycle time period, V_d is the displacement volume, LHV is the fuel lower heating value, AFR is the air-fuel ratio, and m_{cy} is the air mass per cylinder.

Table 2. Results for performance parameter variation at the moment just before and after air boosting

Section (*No.*)	P_a (*bar*)	AFR (λ)	$N_{e,t=0}$ (*rpm*)	Gear (*No.*)	m_{cy} (*gm*)		$\dot{v}_{ave}$ (*km/h/s*)		T_e (*Nm*)		*imep* (*bar*)		η_i (%)	
		After			*Before*	*After*	*Before*	*After*	*Before*	*After*	*Before*	*After*	*Before*	*After*
	1.75	2.0	750	1st	2.54	3.20	1.12	1.47	44.0	55.8	11.1	14.1	58.91	59.81
4.1	2.0	2.0	750	1st	2.54	3.65	1.12	1.70	44.0	64.3	11.1	16.2	58.86	60.11
	2.25	2.0	750	1st	2.54	4.11	1.12	1.93	44.0	72.4	11.1	18.2	58.82	60.36
	2.25	2.0	750	1st	2.54	2.58	1.12	1.19	44.0	45.0	11.1	11.3	58.98	59.47
4.2	2.25	2.0	750	1st	2.54	4.11	1.12	1.93	44.0	72.7	11.1	18.2	58.82	60.36
	2.25	3.3	750	1st	2.54	4.21	1.12	1.80	44.0	47.0	11.1	11.8	58.82	63.06
	2.0	2.0	1500	1st	2.53	3.44	1.17	1.59	43.9	60.9	11.1	15.3	59.28	60.11
4.3	2.0	2.0	1500	2nd	2.53	3.59	0.89	1.38	43.9	63.4	11.1	15.9	59.05	60.01
	2.0	2.0	1500	3rd	2.53	3.68	0.57	0.99	43.8	64.8	11.1	16.3	58.85	60.00
	2.0	2.0	1000	3rd	2.53	3.89	0.58	1.07	43.1	67.8	10.8	17.1	57.84	59.62
4.4	2.0	2.0	2000	3rd	2.53	3.42	0.54	0.88	44.1	60.4	11.0	15.2	59.36	60.11
	2.0	2.0	3000	3rd	2.52	2.84	0.46	0.58	43.9	49.6	11.0	12.5	59.11	59.39
	2.0	2.8	1500	1st	2.53	3.49	1.14	1.23	44.1	46.0	11.1	11.6	59.28	61.77
4.5	2.0	2.9	1500	2nd	2.53	3.65	0.90	0.96	43.9	46.1	11.0	11.6	59.05	61.94
	2.0	3.0	1500	3rd	2.53	3.76	0.58	0.63	43.8	46.1	11.0	11.6	58.85	61.97

To better appreciate the results, the data are presented for the moments just before and after air-boosting assistance. In addition, combustion was assumed to be complete. The results show noticeable acceleration improvements for lower-speed cases, which are much better than those at higher speeds, satisfying the main objective. Even with increased IMEP and engine torque, which reduce turbo lag during low-speed transients and positively impact vehicle drivability, the resulting improvement in thermal efficiency of up to 4% is still, to some extent, moderate. However, the obtained results align very well with what is established in the literature; using a leaner mixture produces less torque and imep but achieves a higher thermal efficiency and leads to less fuel consumption. Thus, achieving better thermal efficiency is possible if the considered technique is integrated with variable-compression-ratio techniques, such as the Miller and Atkinson cycles, which have already proven effective in improving thermal efficiency, particularly under part-load operating conditions.

4. Conclusions

This study investigates the transient performance enhancement of turbocharged direct-injection gasoline engines using air-boosting assistance in the intake manifold. For this purpose, a comprehensive model related vehicle dynamic to gas-exchange processes in the intake and exhaust, turbocharger dynamics, and engine power output was developed. The effectiveness of the boosting assistance, mainly under low- to medium-transient conditions, was clearly demonstrated. This contribution also adds value through modeling, which can be adapted to include transients under higher loads and speeds. The results provide significant insights into the relationships between the dynamic performance of the vehicle and the intake manifold pressure, turbocharger response, and air-fuel ratio. The simulation results are also presented for the drivability performance of the investigated vehicle. The results show that changing the gear ratios at a constant engine speed improves the vehicle transient performance through boosting assistance, even with a reduced fuel flow. This implies that increasing the relative air-fuel ratio while using lower gear ratios along with boosting assistance would result in faster engine and turbocharger acceleration responses. The comparison included three gear ratios (1st, 2nd, and 3rd) and three engine speeds (1000, 2000, and 3000 rpm) to account for the low-to-medium range. In addition, three different boost pressure values (1.75, 2.0, and 2.25 bar) were tested. The results per cylinder showed that the IMEP increased from 11.1 to 18.2 bar and the torque increased from 44 to 72.5 Nm, indicating that a boosting assistance pressure of 2.25 bar achieved

a significant improvement. The results also covered other cases of boosting pressure, engine speed, and relative air-fuel ratio. All results show that IMEP and engine torque either improved or were maintained without fuel addition, but only due to increased manifold pressure, for the moment just before and after the air boosting, especially for lower-speed cases, where compensating for turbo lag during transients will positively impact vehicle drivability. However, the improvement in thermal efficiency of up to 4% is moderate; results could be improved with a leaner mixture or variable-compression-ratio techniques, such as Miller or Atkinson cycles, for part-load operating conditions. Furthermore, the insights show that a small boosting air mass in the range of 5.7–3.4 g and a boost pressure of 2.25 bar give the best acceleration. In addition, they showed noticeable improvements in thermal efficiency and exhaust specific heat ratio values between 1.3484 and 1.3648. These insights can be used for other challenging demands, such as engine downsizing and improving drivability performance.

Acknowledgements
The author would like to express sincere appreciation to colleague Dr. Mohammed H. M. Tamimi from the Department of Linguistics and Translation at Palestine Polytechnic University for his assistance with proofreading the manuscript.

Funding
This study was not supported by any grants from funding bodies in the public, private, or not-for-profit sectors.

Declaration of Competing Interest
The author declares no conflicts of interest.

Credit Authorship Contribution Statement
Momen Sughayyer: Conceptualization; Methodology; Investigation; Validation; Resources; Visualization; Writing-original draft; Writing-review & revise

Availability of Data and Materials
The data supporting the findings of this study are available upon request from the corresponding author.

Ethics Declarations
This study did not involve human participants or animal subjects. Therefore, ethical approval was not required.

Generative Artificial Intelligence Declarations
The authors claim that artificial intelligence-assisted technologies, such as generative AI, were not used to generate content, ideas, or theories. I have utilized AI to enhance the readability and refine the language. I used it under strict human control and supervision. The authors take full responsibility for reviewing and approving the content.

References

[1] IEA, "Global energy review: CO_2 Emissions," Flagship Report, International Energy Agency, Paris, Apr. 2026. [Online] Available: https://www.iea.org/reports/global-energy-review-2026
[2] ICCT, "European vehicle market statistics," Pocketbook 2025/26, International Council on Clean Transportation Europe, Berlin, 2025, [Online] Available: https://theicct.org/european-vehicle-market-statists-pocketbook
[3] N. Zsiga, C. Voser, C. Onder and L. Guzzella, "Intake manifold boosting of turbocharged spark-ignited engines," *Energies*, vol. 6, no. 3, pp. 1746-1763, 2013, https://doi.org/10.3390/en6031746
[4] J. Mamala, K. Praznowski, S. Kołodziej and G. Ligus, "The use of short-term compressed air supercharging in a combustion engine with spark ignition," *International Journal of Automotive and Mechanical Engineering*, vol. 18, no. 2, pp. 8704–8713, 2021, https://doi.org/10.15282/ijame.18.2.2021.08.0664
[5] A. Lefebvre and S. Guilain, "Transient response of a turbocharged SI engine with an electrical boost pressure supply," *SAE Transactions*, vol. 112, no. 4, pp. 1310-1318, 2003, https://www.jstor.org/stable/44742354
[6] S. K. Yadla, D. Terber, J. Keuler and P. Davies, "Secondary air injection with E-Boosting devices," in *15th International Conference on Turbochargers and Turbocharging*, MTZ Worldwide, 2023, https://doi.org/10.1007/s38313-023-1460-5
[7] Á. Bárdos and H. Németh, "Control-oriented air path model for compressed air boosted Diesel engines," *Periodica Polytechnica: Transportation Engineering*, vol. 41, no. 1, pp. 3-12, 2013, https://doi.org/10.3311/PPtr.7093
[8] C. S. Lee and N. J. Choi, "Effect of air injection on the characteristics of transient response in a turbocharged diesel engine," *International Journal of Thermal Sciences*, vol. 41, no. 1, pp. 63-71, 2002, https://doi.org/10.1016/S1290-0729(01)01304-7
[9] S. M. Saad and R. Mishra, "Performance of a heavy-duty turbocharged diesel engine under the effect of air injection at intake manifold during transient operations," *Arabian Journal for Science and Engineering*, vol. 44, no. 6, pp. 5863-5875, 2019, https://doi.org/10.1007/s13369-019-03758-1
[10] L. Shi, X. Zhang, Y. Liu, G. Xiao, M. Ibrahi and, L. Zheng, , "Optimization of electrified turbocharging: Bridging the energy drivability trade-off," *Energy*, vol. 360, Art. no. 141522, 2026, https://doi.org/10.1016/j.energy.2026.141522

[11] O. Vitek, J. Macek, B. Mares, J. Klima and M. Vacek, "Theoretical study of electrically assisted two-stage turbocharger boost system applied to large-bore gas SI ICE," In *WCX SAE World Congress Experience*, Detroit, United States, 2025, https://doi.org/10.4271/2025-01-8354
[12] J. Barman, K. Patchappalam and H. Gambhir, "Compressed air in engine exhaust manifold to improve engine performance and fuel economy," in *SAE Symposium on International Automotive Technology*, Pune, India, 2019, https://doi.org/10.4271/2019-26-0043
[13] K. Subramaniam and W. S.-I. Wan Salim, "Modelling an electrically turbocharged engine and predicting the performance under steady-state engine," *International Journal of Automotive and Mechanical Engineering*, vol. 18, no. 4, pp. 9244-9252, 2021, https://doi.org/10.15282/ijame.18.4.2021.08.0711
[14] K. Subramaniam and W. S.-I. Wan Salim, "Simulation of the performance of an electrically turbocharged engine over an urban driving cycle," *International Journal of Automotive and Mechanical Engineering*, vol. 21, no. 1, pp. 11139–11154, 2024, https://doi.org/10.15282/ijame.21.1.2024.15.0861
[15] T. Ozgur and K. Aydin, "Simulation-based performance analysis of electrically assisted turbocharging in diesel engine," *Processes*, vol. 13, no. 9, p. 2718, 2025, https://doi.org/10.3390/pr13092718
[16] R. Bao and R. Stobart, "Evaluating the performance improvement of different pneumatic hybrid boost systems and their ability to reduce turbo-lag," in *SAE World Congress and Exhibition*, Detroit, United States, 2015, https://doi.org/10.4271/2015-01-1159
[17] S. Kołodziej and J. Mamala, "Analysis of turbocharging pressure in an internal combustion engine using short-term turbocharging," *Applied Energy*, vol. 382, p. 125313, 2025, https://doi.org/10.1016/j.apenergy.2025.125313
[18] O. Kindler, S. Królak, Ł. Warguła and B. Wieczorek, "Research on the design of a non-commercial impulse compressed air supply system for the turbocharger of a spark-ignition internal combustion engine," *Combustion Engines*, vol. 202, no. 3, pp. 11-19, 2025, https://doi.org/10.19206/CE-205010
[19] L. Xia, Z. Yao, Z. Li, H. Wang, Y. Li, Z. Zheng and M. Yao, "Experimental study on thermal efficiency improvement of highly premixed charge combustion engine with high compression ratio chamber," *Fuel*, vol. 422, Art. no. 139163, 2026, https://doi.org/10.1016/j.fuel.2026.139163
[20] N. F. Al-Muhsen, G. Hong and F. B. Ismail, "Performance of combustion and emissions characteristics of ethanol dual injection spark ignition engine," *International Journal of Automotive and Mechanical Engineering*, vol. 18, no. 3, pp. 9082-9089, 2021, https://doi.org/10.15282/ijame.18.3.2021.20.0697
[21] V. Ravaglioli, G. Silvagni, F. Ponti, N. Cavina, A. Brusa and M. De Cesare, "Development of a control-oriented physical model for cylinder pressure peak estimation in SI engines," *International Journal of Engine Research*, vol. 26, no. 1, pp. 101-117, 2025, https://doi.org/10.1177/14680874241272904
[22] H. Arslan, "Thermodynamic analysis for improving the efficiency of SI engine at part-load conditions," *Applied Thermal Engineering*, vol. 279, no. F, Art. no. 127983, 2025, https://doi.org/10.1016/j.applthermaleng.2025.127983
[23] E. Wenz, A. Pauls, M. Thielen, A. Todt and P. Eilts, "Exploiting SI engine efficiency through lean burn operation in combination with stroke extension, Miller timings and high compression ratios," in *15th International Conference on Engines and Vehicles*, Capri, Italy, 2021, https://doi.org/10.4271/2021-24-0034
[24] G. Conway, A. Joshi, F. Leach, A. García and P. K. Senecal, "A review of current and future powertrain technologies and trends in 2020," *Transportation Engineering*, vol. 5, Art. no. 100080, 2021, https://doi.org/10.1016/j.treng.2021.100080
[25] L. Guzzella and C. H. Onder, *Introduction to modeling and control of internal combustion engine systems*, Second Edition, Zürich, Switzerland: Springer-Verlag Berlin Heidelberg, 2010.
[26] J. B. Heywood, *Fundamentals of internal combustion engines*, Second Edition, New York, United States: McGraw-Hill Education, 2018.
[27] R. S. Benson, *The thermodynamics and gas dynamics of internal-combustion engines*, First Edition, Vol. 1, Oxford, UK: Clarendon Press, 1982.
[28] C. R. Ferguson and A. T. Kirkpatrick, *Internal combustion engines: applied thermosciences*, Third Edition, West Sussex, UK: John Wiley and Sons, Ltd, 2016.
[29] P. Moraal and I. Kolmanovsky, "Turbocharger modeling for automotive control applications," In *SAE International Congress and Exposition*, Detroit, United States, 1999, https://doi.org/10.4271/1999-01-0908
[30] T. D. Gillespie, *Fundamentals of vehicle dynamics*, International Revised Edition, Warrendale, United States: SAE International, 2021.
[31] W. Duan, X. Geng, S. Zhang, L. Wang and J. Pan, "Lean combustion effects on a high-compression methanol SI engine derived from a turbocharged Miller cycle gasoline engine", *Advances in Mechanical Engineering*, vol. 17, no. 10, pp. 1- 13, 2025, https://doi.org/10.1177/16878132251383368
[32] A. Ferrari and P. Pizzo, *Injection technologies and mixture formation strategies for spark-ignition and dual-fuel engines*, First Edition, Warrendale, United States: SAE International, 2022.
[33] F. Aydın and İ. Kırmaz, "Effects of gasoline and LPG on the performance and emissions of a turbocharged direct-injection vehicle: a response surface methodology approach," *International Journal of Automotive and Mechanical Engineering*, vol. 22, no. 4, pp. 12872–12886, 2025, https://doi.org/10.15282/ijame.22.4.2025.3.0980